Experimental and CFD study of a new one-pot reactor for hybrid catalysis

Myriam Frey, Léo Violet, Dominique Richard, Pascal Fongarland

Version of Record: https://www.sciencedirect.com/science/article/pii/S138589471932368X
Manuscript_e4aedf8ee2a82350e0f2df0462588bac

Experimental and CFD study of a new one-pot reactor for hybrid catalysis.

Myriam Frey[a], Léo Violet[a,1,*], Dominique Richard[a,2,**], Pascal Fongarland[a]

[a] *Laboratoire de Génie des Procédés Catalytiques (UMR 5285, CNRS, CPE Lyon, UCB Lyon 1), Université de Lyon, 3, rue Victor Grignard F-69616, Villeurbanne, cedex*

Abstract

A new reactor design is proposed to carry out hybrid catalysis. It involves a two-basket reactor, one filled with an heterogeneous catalyst and the other with a supported enzymatic catalyst The physical transfer properties (k_La, mixing time,...) have been studied experimentally and the velocity, mixing time and thermal behavior simulated by CFD. Volumetric oxygen mass transfer (k_La) between $0.02\,s^{-1}$ and $0.035\,s^{-1}$ are obtained. The simulated mixing times are in good agreement with the experimental ones. The mass flow field are simulated in various conditions of stirring. The thermal behavior of the reactor is also simulated, allowing for the observation of two zones (cold and hot) with a ΔT of up to 15 K while keeping good mass transfer characteristics.

Keywords: Hybrid catalysis, one-pot, basket reactor, mixing time, k_La, CFD

*corresponding author
**corresponding author
Email addresses: lev@lgpc.cpe.fr (Léo Violet), dri@lgpc.cpe.fr (Dominique Richard)

1. Introduction

The use of enzyme for fine chemicals production has been the subject of many researches over the last decade. In this context, the recent concept of hybrid catalysis emerged: a coupling of chemical and enzymatic catalysis [1–4]. The aim the Glycybride project is to convert glycerol into valuable chemicals (target reaction) by taking advantage of the synergy between enzymatic and heterogeneous catalysis. The heterogeneous catalysis step involving an oxidation by O_2, catalyzed by supported noble metal. In order to design a one-pot reactor able to perform three phase hybrid catalysis, part of the challenge lies in the different reaction conditions (temperature, stirring speed, oxygen concentration) required by heterogeneous and enzymatic catalysis. The pros and cons for the combination of chemo- and biocatalytic reactions have been presented by Rudroff *et al.* in a recent review [5]. The advantage of a one-pot based process, is that it does not require any treatment between the two reaction step since they are run simultaneously, provided that the chemical compatibility of the reaction medium is ensured.

The design of the reactor must allow to work under different conditions, which means having a temperature and/or oxygen concentration gradient, as well as different stirring speed for each catalyst. For this purpose we propose a two basket reactor, each one filled with the appropriate catalyst, either supported enzyme or heterogeneous catalyst. The upper part of the reactor, around the upper basket will benefit of a high O_2 content, due to a

self-suction turbine and will be heated to a temperature as high as possible to ensure a high oxidation rate, but compatible with an enzyme-bearable temperature in the bottom part. The lower part, around the lower basket containing a supported enzyme will require only moderate stirring and will be kept at a temperature below 60 °C. The chemical compatibility of the reaction medium has been checked in the case of a model reaction and is reported in a previous paper [6].

Very few studies have been reported so far on the characterization of basket reactors [7–10]. Warna *et al.* [7] were the first to report the use of CFD to study the flow rate of fluid over the catalyst particles in a rotating basket reactor. Magnico and Fongarland [8] studied two stationary catalytic basket stirred tank reactors of different geometry by means of CFD and observed a good agreement with the experimental data (PIV and mass transfer measurements). They showed that the same mass transfer properties could be obtained through two different local velocity patterns and two different porous media. More recently Santos-Moreau *et al.* [9] investigated the liquid flow field in a stirred reactor, with catalyst particles contained in a fixed basket, by means of CFD RANS (Reynolds-Averaged Navier–Stokes) simulations. They showed from these calculations that there is a recirculation pattern in the basket and a non-uniformity of velocities inducing differences in mass transfer coefficients in the catalytic basket. So far no two-basket reactor has been reported in the literature and no study of such reactor with either experiment or simulation tools.

We aim at developping a synergy between enzymatic and heterogeneous catalysis in a one-pot reactor in order to valorize biomass. Our aim is to design a one-pot reactor able to perform three phase hybrid catalysis [1], one step being an oxidation and the other an enzyme-catalyzed reaction. A model hybrid catalysis reaction coupling enzymatic and heterogeneous catalysis has been studied in a slurry reactor [6], our aim being to transpose this study in a new reactor to improve the performances as compared with a slurry one. Knowing that enzyme and heterogeneous catalysis require different reaction conditions, such as temperature, stirring speed, oxygen concentration (oxygen possibly inhibiting the enzymatic reaction) we designed a reactor allowing for the separation of the two kind of catalysts and possibly for the presence of two zones in a one-pot reactor. The object of the present work is to study the hydrodynamics, and possibly the thermics of such a new two-basket reactor.

In the present work, a CFD-based modeling of the proposed two-basket reactor is performed, in order to investigate its mixing time, mass transfer coefficient and thermal behavior. This study is completed by an experimental characterization of the reactor in order to validate the model: volumetric mass transfer coefficient, mixing time and residence time distribution.

Nomenclature

C tracer concentration ($\mathrm{g\,L^{-1}}$)

C^* reduced concentration (dimensionless)

D_{eq} equivalent diameter (mm)

k_La volumetric O_2 mass transfer coefficient ($\mathrm{s^{-1}}$)

L characteristic lenght (meter)

N stirring rate (rpm)

Δp pressure drop (Pa)

Q flow rate ($\mathrm{L\,min^{-1}}$)

Sc_t turbulent Schmidt number (dimensionless)

t time (s)

T temperature (K)

$|u|$ velocity ($\mathrm{m\,s^{-1}}$)

Greek letters

α permeability ($\mathrm{m^2}$)

β viscous resistance ($\mathrm{m^{-1}}$)

ϵ porosity (dimensionless)

ϕ sphericity (dimensionless)

μ viscosity (Pa s)

θ mixing time (s)

ω stirring rate (rpm)

Indexes

inf relative to the lower part

L relative to the liquid phase

sup relative to the upper part

Exponents

0 initial value (tracer concentration)

basket relative to a basket

cooler relative to a cooler in the reactor

eq equilibrium value (tracer concentration)

wall relative to a wall of the reactor

2. Experimental section

2.1. Reactor geometry and equipments

The reactor tank is a cylinder of 10 cm in diameter and 20 cm in height. The reactor is fitted with two superimposed annular baskets of equal dimension (inner diameter 5.2 cm, outer diameter 7.2 cm, height 6.3 cm). The baskets are separated by an interval of 5 cm. The stirring is carried out using a Parr-type stirring device (see photograph in reference [11]) located inside the upper annular basket. The reactor is fitted with a three-points thermocouple for temperature measurement between the basket and the wall of the tank at three different heights: the middle of each basket and the middle of the space between the baskets. A coil for temperature exchange can be added inside the reactor as discuted later (*cf.* section 3.2). A schematic view of the reactor is presented in figure 2.

2.2. Methods for the characterization of the reactor

2.2.1. k_La measurements

The dissolved O_2 concentration was measured with an Orbisphere Model M1100 Sensor and Model 410 Analyzer from Hach. The k_La were calculated using the dynamic method reported by Garcia-Ochoa et al [12]. The probe can be positionned at 3 height in the reactor wall (*cf.* figure 1a). By switching a gas flow through the gaseous sky of the reactor from nitrogen to air, the

O_2 concentration decreases according to equation 1.

$$\ln\left(\frac{C_L^0}{C_L}\right) = k_L a \cdot t \tag{1}$$

Conversely switching back to air increases the concentration of dissolved O_2 according to equation 2.

$$\ln\left(1 - \frac{C_L}{C_L^{eq}}\right) = -k_L a \cdot t \tag{2}$$

The linearization of both relations allows for the determination of the volumetric mass transfer coefficient $k_L a$.

2.2.2. Mixing time measurements

The tracer used for the mixing time measurement is NaCl.10 mL of a satured solution are injected and the evolution of the conductivity is monitored through a conductimetry probe which can be positionned at 3 different height along the reactor wall (*cf.* figure 1b). The mixing time is defined according to the proposition of Kasat *et al.* [13], as the time θ_{mix} when the reduced concentration $C^*(\theta)$, defined in equation 3, reach the value 1 ± 0.05 depending of the probe position (*cf.* figure 12) .

$$C^*(\theta) = \frac{C(\theta) - C(\infty)}{C(0) - C(\infty)} \tag{3}$$

2.2.3. Residence time measurements

The setup used is presented in figure 1c, the tracer used is NaCl (saturated aqueous solution) and the amount injected 10 mL . The conductivity at the outlet of the reactor is monitored to obtained the residence time of the tracer.

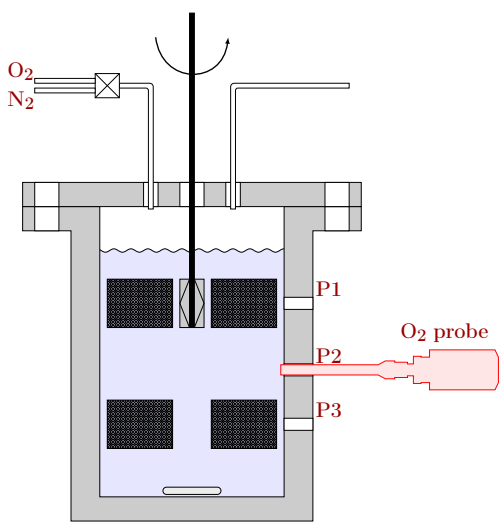

(a) k_La measurement

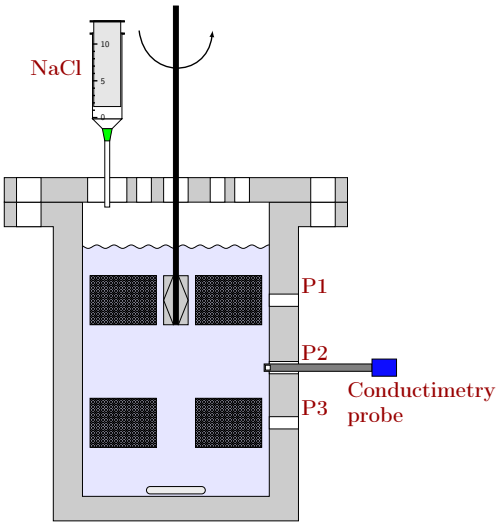

(b) mixing time measurement

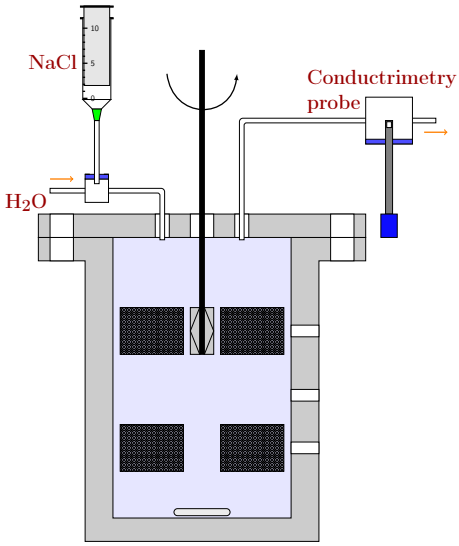

(c) RTD measurement

Figure 1: Experimental setups for the physical characterization of the reactor

2.3. Materials and methods for CFD Modelling

For the first part of the study, ANSYS Fluent® software was used to perform CFD modeling. Hydrodynamic and then mixing properties were modeled for Liquid/Solid system. Then, the energy balance was added to model the temperature gradient that can be obtained under different conditions (heating system, stirring, presence of catalytic basket, etc.).

2.3.1. Reactor geometry and meshing

Reactor geometry imported from SolidWorks® file is simplified and prepared for CFD simulation in SpaceClaim® software included in Fluent® license. The final geometry (Figure 2) is composed of the two catalytic baskets, two heat exchanger coils, the upper impeller without shaft and a magnetic barrel. Coils and stirring bar presence are optional in the experimental reactor and also in the CFD geometry. ANSYS Meshing® is used for the meshing. A uniform cell size is used for all the fluid volumes and meshing dependency was tested with 3.9, 5.9 and 8.7 millions of mesh cells. All give similar results so 3.9 millions mesh cells was finally selected to reduce calculation times.

2.3.2. Modeling the flow

Realizable $k - \epsilon$ turbulence model associated to Multiple Reference Frame (MFR) model to deal with rotating parts is the more spread model combination and well represent flow in stirred tank reactors [14–17], including works with catalytic baskets [8, 9, 18]. Although the turbulent transport is known to be dependent upon the chosen value for the turbulent Schmidt number

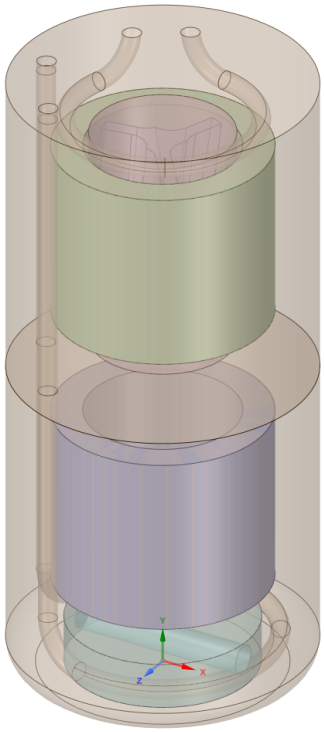

Figure 2: Reactor geometry in Fluent®

Sc_t [10, 19] the study of the dependancy was not carried out and the default value of 0.7 was assumed instead. The gain in precision with more complex models as LES type for turbulence, or Sliding Mesh for rotating parts do not compensate the hight calculation needs of these last methods. In fact, estimation to global characteristics of the flow as power number or mean velocity gives very satisfactory results with $k - \epsilon$ and MFR model association [20, 21].

The MFR method is a steady state approximation in which the fluid domain is divided in several zones with different reference frames, cylindrical zones around the moving parts (impellers, magnetic stirrers) and stationary zones containing the static parts (baffles, coils, reactor walls). In the static zone, the equations keep their classic form while in the rotating zone the equations are modified to incorporate acceleration terms due to the transformation from stationary to moving reference frame. At the interface between zones, local reference frame transformations enable to use variables of one zone as boundary conditions of the adjacent zones. The two catalytic baskets are modeled as porous media [22] in which fluid flow is solved using Darcy-Forchheimer law (eq. 4). To do so, each basket needs to be characterized by its porosity ϵ, permeability α and viscous resistance β. Porosity is experimentally estimated while α and β are calculated using the Ergun relations (eq. 5 et 6). Table 1 presents the estimated properties for the various catalytic supports used in this study.

$$\frac{|\Delta p|}{L} = \frac{150\mu}{\alpha}|u| + 1.75\rho\frac{\beta}{2}|u|^2 \tag{4}$$

$$\alpha = \frac{D_p^2}{150}\frac{\phi^2\epsilon^3}{(1-\epsilon)^2} \tag{5}$$

Table 1: Catalytic basket characteristics

Catalytic support	Shape (sphericity)	D_{eq} (mm)	Porosity ϵ (dimensionless)	Permeability α (m^2)	Viscous resistance β (m^{-1})
Titane dioxide	cylinder (0.72)	4.24	0.72	4.295×10^{-7}	713.7
Active carbon	spherical (0.9)	3.38	0.4	1.547×10^{-7}	1850
Glass	spherical (1)	0.46	0.38	2.036×10^{-7}	85500

$$\beta = \frac{3.5}{D_p} \frac{(1-\epsilon)}{\phi \epsilon^3} \tag{6}$$

Finally, all walls are defined as surfaces with no-slip conditions while the top of the reactor, assimilated to the liquid surface, is defined as wall with zero shear stress. The Menter Lechner near-wall treatment, a y^+ insensitive method, has been used for modelling the boundary layers.

2.3.3. Numerical methods

Continuity and momentum equation are solved using Semi-Implicit Method for Pressure-Linked Equations (SIMPLE) algorithm and the following discretization schemes: PRESTO! for pressure and second order upwind for the other equations. PRESTO! scheme is well adapted to swirling flows and flows involving steep pressure gradients as porous media [23], while 2^{nd} order scheme give more accurate results than 1st order ones for stirred tanks [20].

Residuals convergence limits are decreased at 1×10^{-5} except for energy equation kept at its default value at 1×10^{-6}. However convergence is more accurately checked following the evolution with iterations of characteristic

variables of the system: average magnitude of velocity and tangential velocity; torques resulting on pressure and friction forces on impeller, magnetic stirrer and reactor wall; average dissipation rate constant ϵ; and average temperature in the reactor. Convergence criterion is the stabilization of all these values with iterations.

3. Results and discussion

3.1. Physical characterization of the reactor

3.1.1. k_La measurements

Figure 3 shows the increase of the measured k_La value with the stirring rate. Values of $0.035\,s^{-1}$ are obtained for the highest rate when the probe is the position closest to the gaseous sky. For the probe positions deeper in the liquid a value of $0.02\,s^{-1}$ is obtained. Some values reported in the literature for stirred tank reactors, with various type of impellers, including or not oxygen bubbling and the present of a basket filled with catalyst are presented in table 2.

The values of k_La achieved are close to those generally reported for similar reactor, espacially with the Parr turbine [11, 26] and slightly lower than the values reported with Rushton turbines and air bubbling.

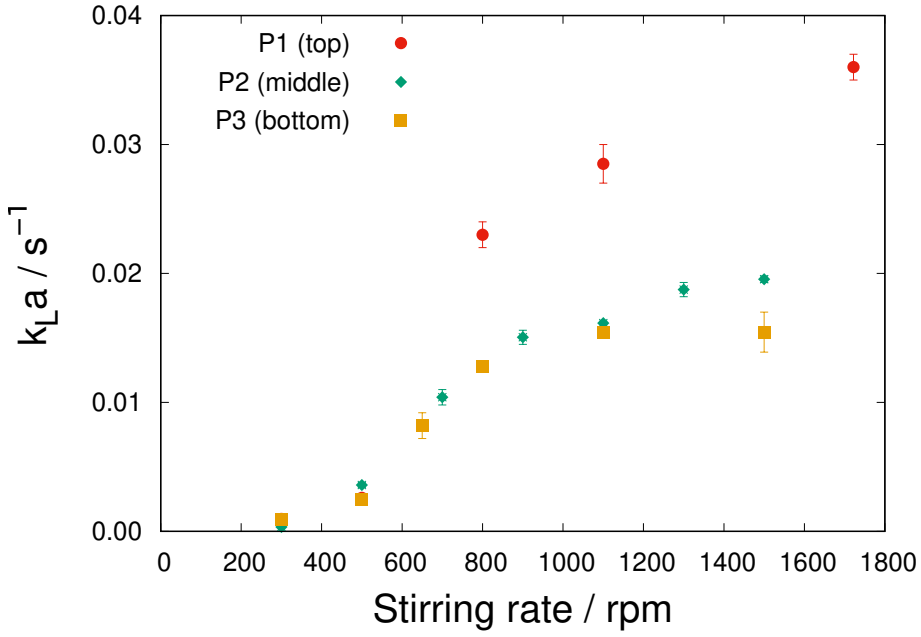

Figure 3: k_La as a function of the stirring rate for the different probe positions: P1 probe at the height of the upper basket, P2 probe between the baskets, P3 probe at the height of the lower basket.

Table 2: Some values of k_La reported in the litterature

Agitation mobile	Stirring rate	Gas bubbling	V_G $m\,s^{-1}$	Basket	k_La s^{-1}	Reference
Rushton turbine (single)	1000	yes		no	0.045	[24]
Rushton turbine (twin)	1000	yes		no	0.055	[24]
Rushton turbine	1200	yes	0.01	no	0.1	[25]
Parr mobile	1000				0.0013	[26]
AE[a] mobile	1000				0.0023	[26]
Parr mobile	1500		0.08	yes		[11]
AE mobile	1000			0.02	yes	[11]

[a]Autoclave Engineers

3.1.2. Mixing time measurements

The mixing time have been measured for different positions of the probe (P1 at z= 16.9 cm relative to the bottom of the tank, P2 at z= 11.5 cm and P3 at z= 6.1 cm). No effect of the angular position of the injecting point relative to the probe position is observed. As can be seen on figure 13, the experimental mixing time decreases rapidly when the stirring rate increases from 300 rpm to 500 rpm. For values of the stirring rate above 500 rpm, the variation of the mixing time is not significant.

3.1.3. Residence time distribution

Experimental Residence Time Distributions have been measured and compared with the simulated ones of an ideal CSTR. Figure 4 shows the $E(t)$ curve for both and indicate a good agreement.

3.2. CFD results

Two reactor geometries have been studied.

Case 1: coils and magnetic bar are not included, and the upper catalytic material is titanium oxide pellets. These conditions correspond to the mixing time experiments previously implemented.

Case 2: coils and magnetic barrel are added and the upper catalytic material is replaced by platinum on carbon grains, these conditions fitting to future experimental conditions.

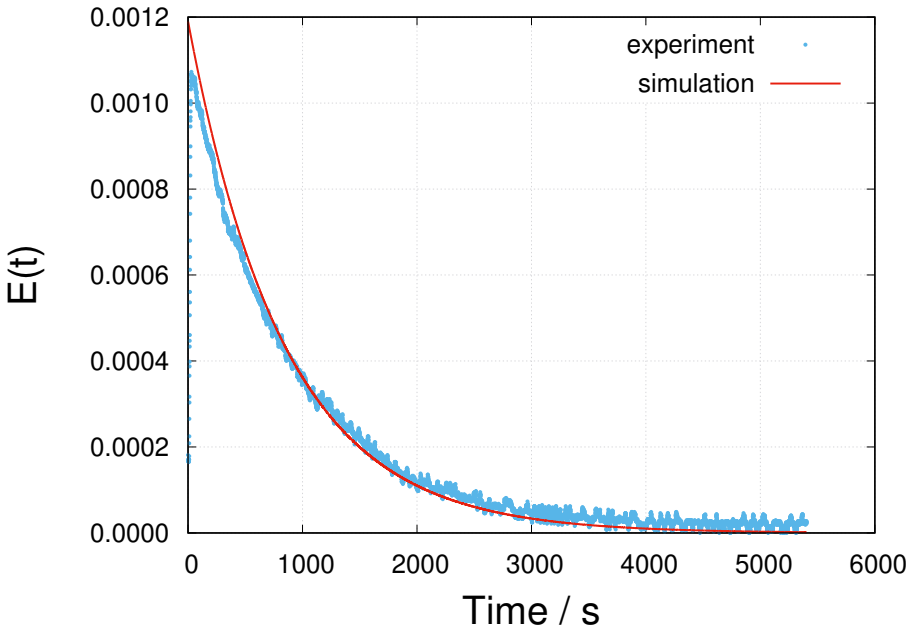

Figure 4: Residence time distribution $E(t)$ curves: experimental curve at a flow rate Q =0.1 L min^{-1} and a stirring rate of the Parr agitation mobile $\omega = 500$ rpm compared with simulated curve.

Results about flow fields, mixing time estimation and heat exchanges are successively presented below. In the Flow section 3.2.1, results on the two reactor configurations (case1, case 2) are presented and will be each time clarified.

3.2.1. Flow

Two main aspects have to be evaluated concerning the flow fields: the flow conditions in each basket and the "transfer" between the upper and lower regions of the reactor. Figure 5 shows average velocity magnitude for the

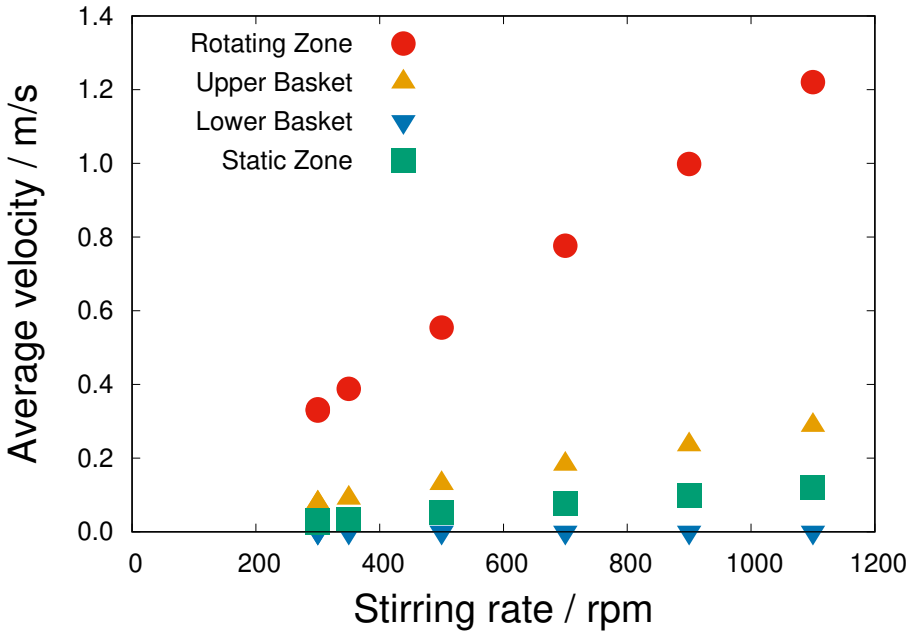

Figure 5: Average velocity magnitude in the different zones of the reactor for case 1.

different characteristic parts of the reactor for various stirring rates of the impeller (in absence of coils and magnetic bar). The high velocity in the

Table 3: Reynolds numbers at different stirring rates

	Impeller stirring rate (rpm)	Magnetic bar stirring rate (rpm)	Re upper basket	Re lower basket
case 1	300	-	508	0.005
	700	-	1027	0.015
	900	-	1322	0.03
case 2	900	300	808	0.50
	900	450	809	0.65

fluid region around the impeller is highlighted with velocity magnitude from $0.4\,\mathrm{m\,s^{-1}}$ to $1.2\,\mathrm{m\,s^{-1}}$. Then the upper basket seems to break the flow since average velocity is about $8\,\mathrm{cm\,s^{-1}}$ to $29\,\mathrm{cm\,s^{-1}}$ in this basket and slower in the other parts of the reactor. Figure 8 and Figure 11 giving the fields of velocity magnitude well illustrate this point. Particle Reynolds number (Equation 7) can be calculated from velocity and basket characteristics. Estimated values in Table 3.

$$Re_p = \frac{\rho u d_p}{\mu(1-\epsilon)} \tag{7}$$

where ρ is the fluid density, u the average superficial velocity of the fluid in the basket, μ is the fluid dynamic viscosity, d_p the particle diameter and ϵ the void fraction of the basket.

Reynolds numbers illustrate how different are the flow conditions in the different baskets. The impeller ensures a transitory flow ($Re_p > 200$) in the upper basket, but it can locally increase to 5000 even at low stirring speed, at the entrance of the basket from the impeller zone, leading to turbulent flow in this region. On the contrary, clear laminar conditions are observed in

the lower basket.

Also, it appears that the change of catalyst shape (from TiO_2 cylender to C grains) decreasing the porosity reduces the average velocity magnitude in the upper part, as the reduction of the Reynolds number can illustrate it. Figure 6 shows the mass pumping rate of the impeller, corresponding on the

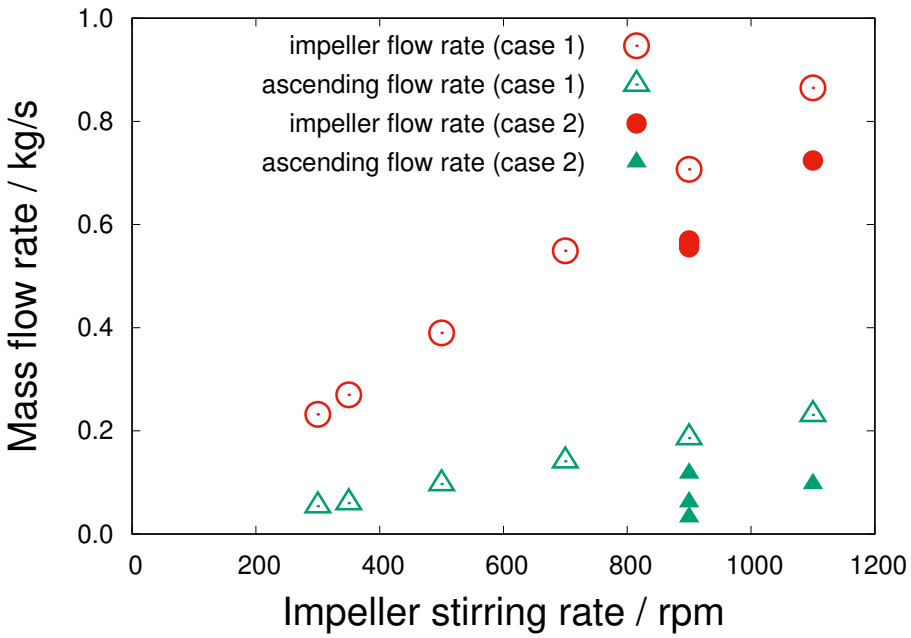

Figure 6: Mass pumping rate of the impeller (blue) and mass exchange rate between upper and lower part of the reactor

fluid flow rate dragged away by the moving body, and exchange mass flow rate between upper and lower part of the reactor. The figure highlights how low is the transfer between the two zones compared to the pumping power on the impeller. This suggests an important recirculation flow in the upper zone and then the partial segregation of the fluid, exactly the expected behavior

in this reactor. Flow and velocity fields in the next figures will support this assumption.

The following observations can be made on the velocity fields from Figures 7 to 10:

1. From the impeller zone, the fluid is radially expelled through the upper basket, and then main recirculation loops carry the fluid along the reactor wall before to bring it back to the impeller zone from the top or the bottom of the inner space of the upper basket.
2. A minor fraction of the fluid (with flow rate estimated in Figure 6) goes to the lower part of the reactor. The fluid goes down in the inter space between reactor wall and the lower basket.
3. Recirculations carry the fluid from the inner region to the outer one to go up along the reactor wall, helped by the magnetic impeller at the bottom.
4. Finally a minor part of the fluid goes through the lower basket from the outer to the inner side.

Finally, the streamlines in Figure 11 illustrate once more the fluid segregation between upper and lower part of the reactor. To conclude about the flow, the potential to create two separated reactive zones seems very promising. However two contradictory matters should be evaluated: (1) the temperature fields (2) the transport limitations. Indeed, the flow conditions presented below have to be optimal enough to create two temperature zones as clear as the two hydrodynamic zones, and at the opposite, it has to be checked

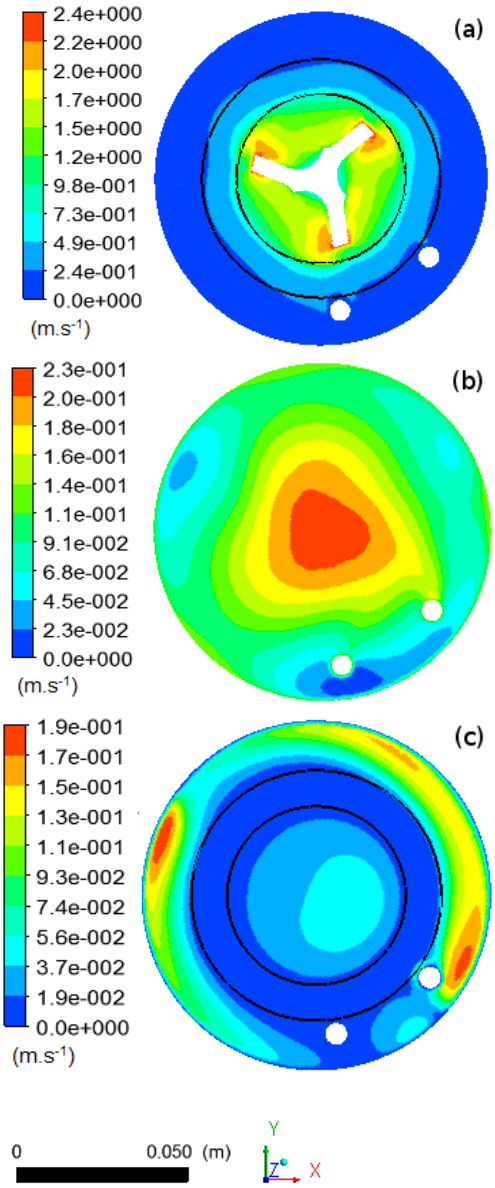

Figure 7: Velocity magnitude on 3 horizontal plans at a) $z = 16.9\,\text{cm}$ (mid impeller and upper basket level), b) $z = 11.5\,\text{cm}$ (inter basket level), and c) z =6.1 cm (mid lower basket level) where the height z is relative to the bottom of the reactor tank. The black lines represent the upper and lower basket limits. Stirring rates at 1100 rpm for the impeller, 300 rpm for the magnetic barrel, coils are present.

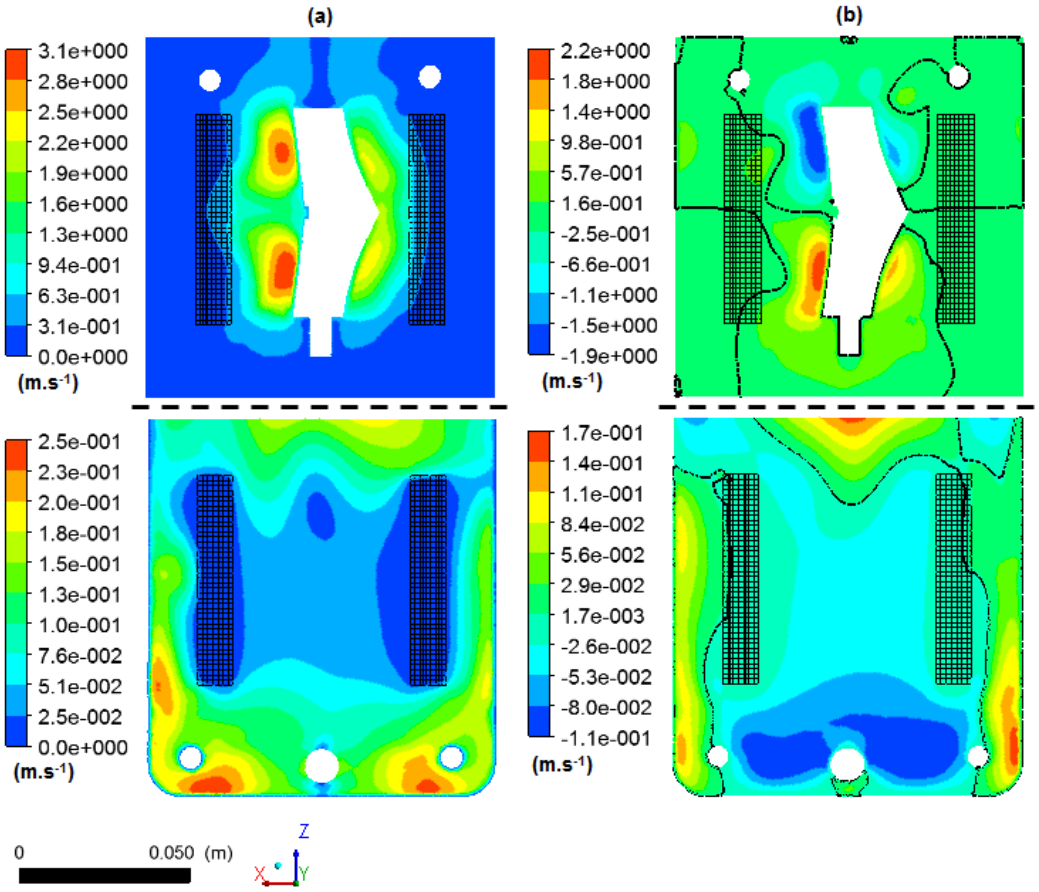

Figure 8: Velocity magnitude (a) and axial velocity magnitude (b) on a vertical plan of the reactor at y = 0. Black line in Figure 8b represents the iso-value $u_z = 0\,\mathrm{m\,s^{-1}}$. Stirring rates at 1100 rpm for the impeller, 300 rpm for the magnetic barrel, coils are present.

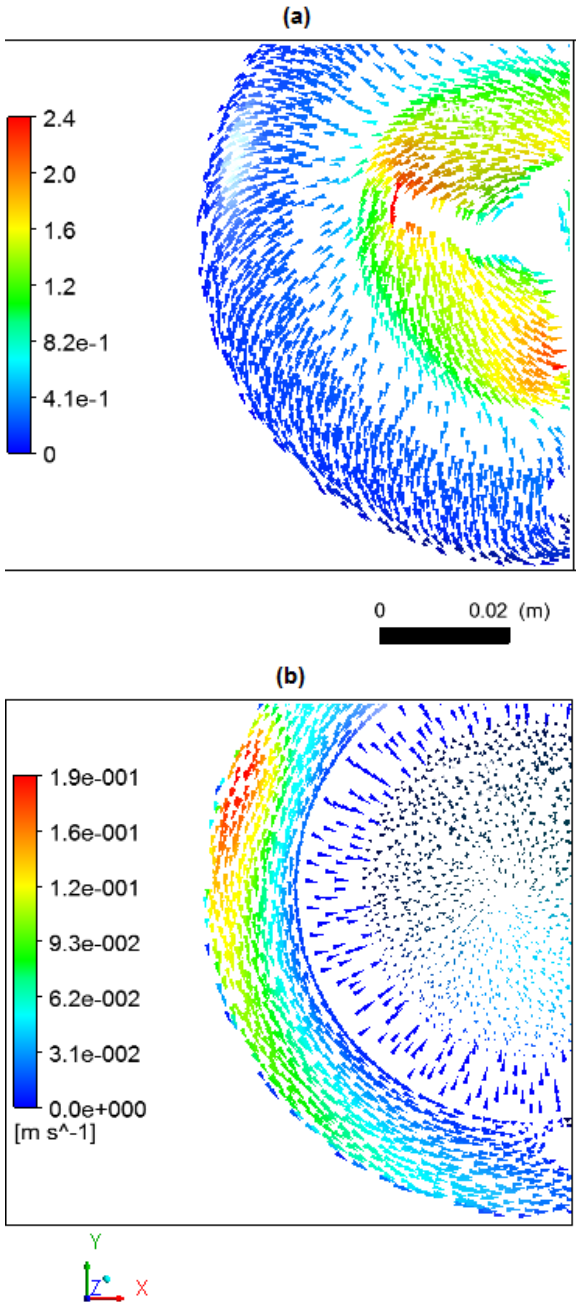

Figure 9: Flow fields on horizontal plans at $z_1 = 16.9\,\text{cm}$ (a) (impeller and upper basket) and $z_3 = 6.1\,\text{cm}$ (b) (lower basket). Vector length is normalized. Stirring rates at 1100 rpm for the impeller, 300 rpm for the magnetic bar, coils are present.

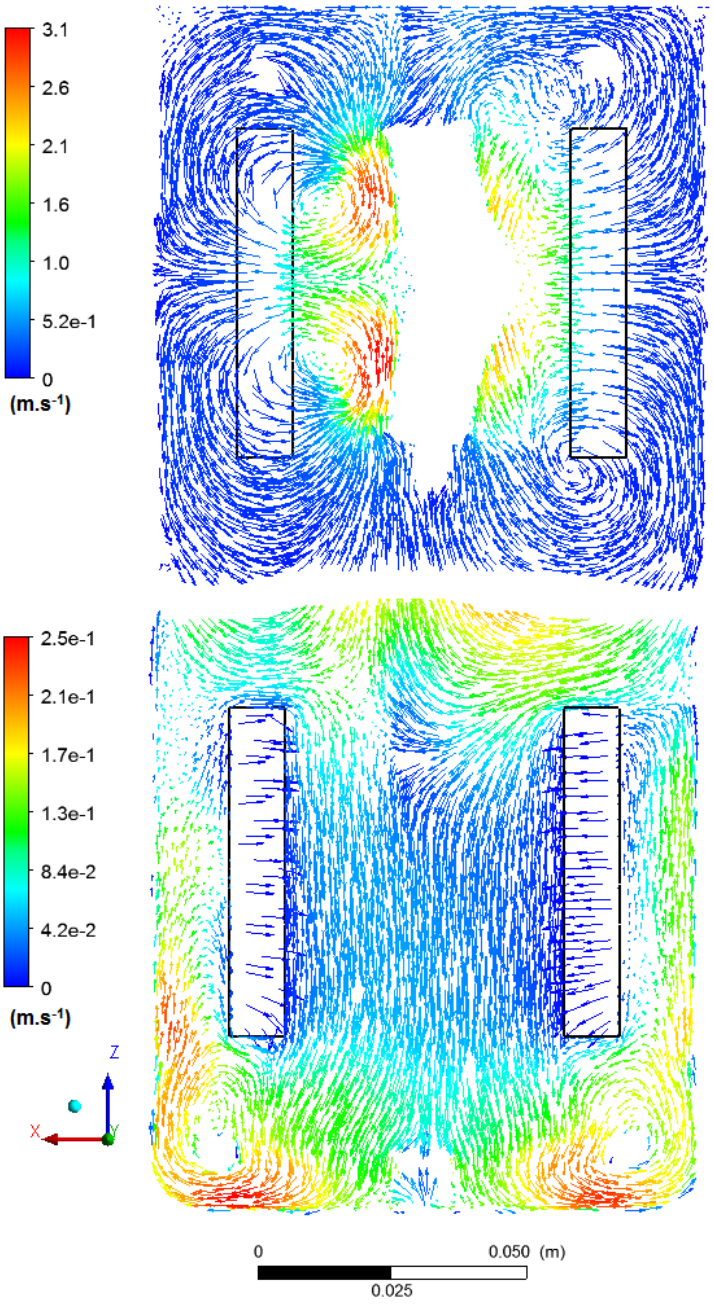

Figure 10: Flow fields on a vertical plan at y = 0 cm. Vector length is normalized. Stirring rates at 1100 rpm for the impeller, 300 rpm for the magnetic bar, coils are present.

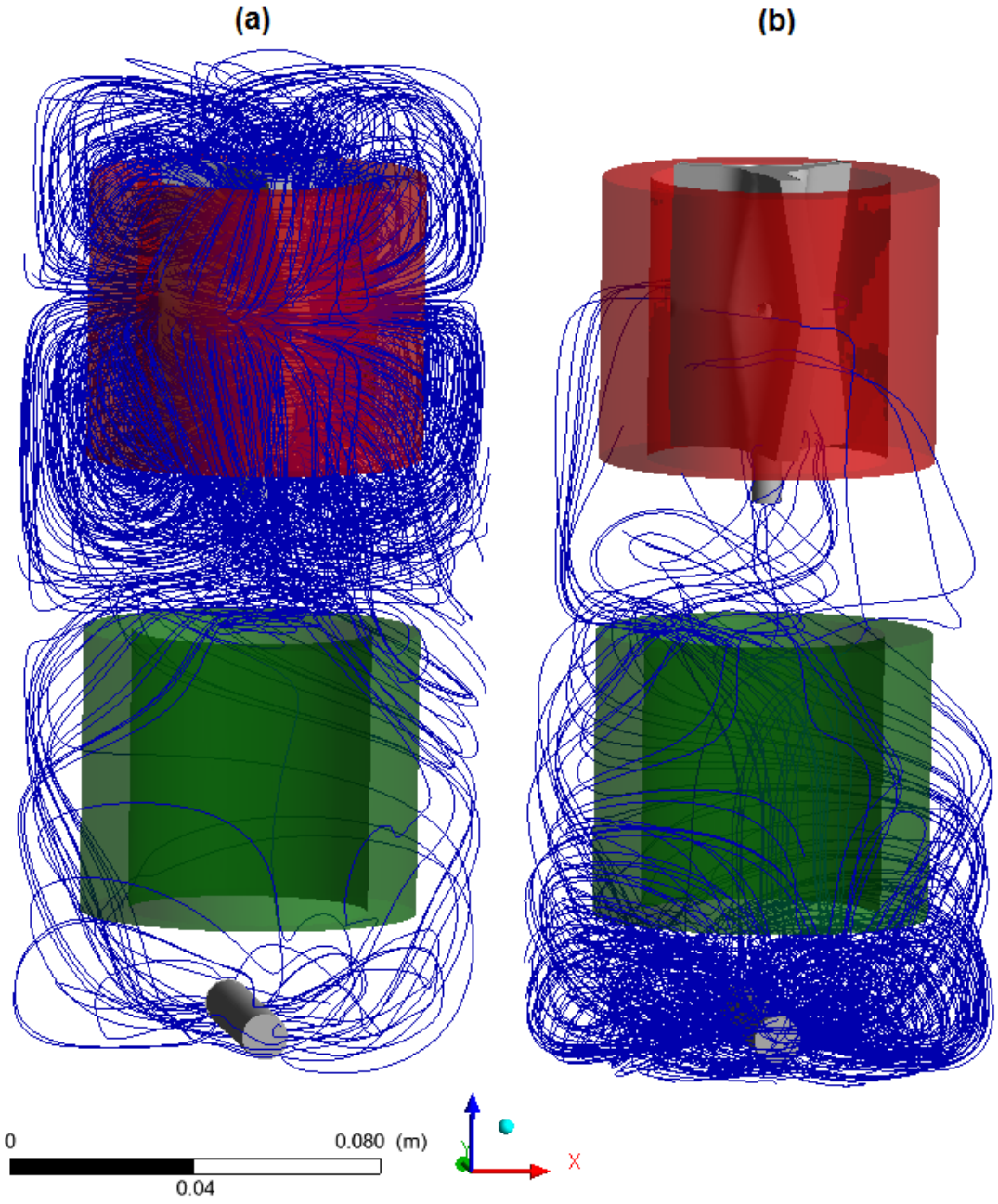

Figure 11: Streamlines starting from the impeller zone (a) and the magnetic stirrer zone (b).

if the very low velocity conditions created in the lower basket do not limit mass transfer. The first point is evaluated in section 3.2.3.

3.2.2. Mixing time

To validate CFD simulations, we propose to compare estimation of mixing time estimated with the CFD model and the ones experimentally estimated (section 3.1) To estimate mixing time with CFD simulation, the following procedure is used:

(a) Hydrodynamics equations are solved with stationary method (MRF) in a first step.

(b) Model to solve equations for species transport and mixing must be added, while the option to solve flow and turbulence equation must be deselected. In this way, species transport equations can be solved independently.

(c) A "tracer" species, with the same properties than the solvent, is created. A patch for initialization of the tracer mass fraction in the reactor is added in a spherical volume at the top of the reactor. It corresponds to an "injection" zone.

(d) The species transport equations are solved in transient mode. Evolution of the tracer mass fraction is then monitored regarding time in three different point of the reactor corresponding to the height of the three positions for the conductimetric probe of the experimental reactor (*cf.* section 2.2.2).

Examples of simulations are shown in Figure 12.

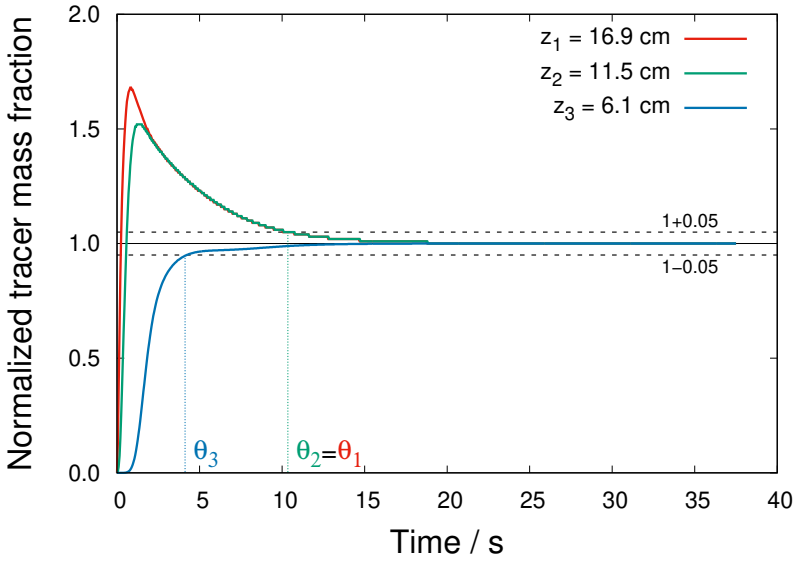

Figure 12: Numerical monitoring of tracer normalized mass fraction at points at 3 different axial positions: $z_1 = 16.9$ cm (impeller and upper basket level), $z_2 = 11.5$ cm (inter basket level) and $z_3 = 6.1$ cm (mid lower basket level). Stirring rates at 1100 rpm for the impeller (case 1).

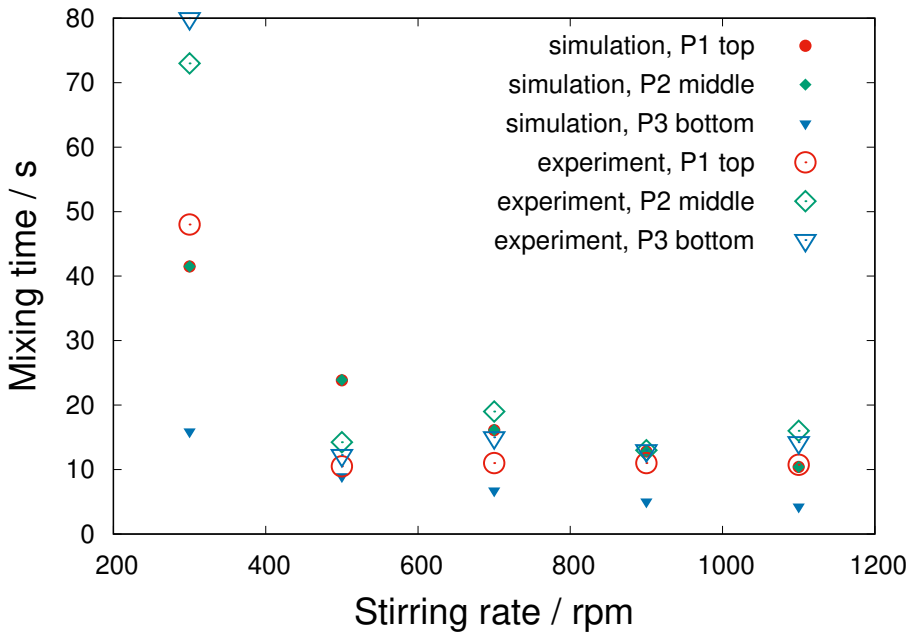

Figure 13: Comparison of the mixing time either a) derived from CFD simulation (filled markers), or b) measured experimentally (empty markers) at different heights in the reactor. P1 top at $z_1 = 16.9$ cm (impeller and upper basket level), P2 middle at $z_2 = 11.5$ cm (inter basket level) and P3 at $z_3 = 6.1$ cm (lower basket level)

Mixing time is defined as the time when 95% of the equilibrium mass fraction value is reached. Figure 13 shows the influence of the stirring rate of the impeller on the mixing time for the CFD simulations as well as for the experimental measurements.

The comparison of mixing times obtained from CFD simulation and experimental measurement shows:

for CFD simulation: The mixing time continuously decreases when the stirring rate increases. For the two upper captor positions (P1 and P2), values are very close while for the lower position (P3) the mixing time is significantly lower as could be expected from the curves presents in Figure 12.

for experimental measurement: The mixing time sharply decrease between 300 and 500 rpm and doesn't change much for higher values of the strirring rate. Values are very close wherever the captor position above 500 rpm, while at 300 rpm they are position dependant

Indeed for the upper positions of the captor, the mixing time pattern are similar between the experimental and simulation value, even if they may be different at the lowest stirring rate they tend to become closer for the highest stirring rate. At contrary for the lower captor position, the experimental values are always above the ones issued from simulation even at the highest stirring rate. This means that the simulation probably overestimates the diffusion rate of the tracer in the lower part of the reactor.

3.2.3. Thermal behavior

In this part, energy equations are also solved. On the experimental reactor, two independent double walls and two independent coils, one series for the upper part and another for the lower part, can assure the heat exchange. In the CFD model, the reactor walls and coils are simple surfaces on which constant temperature or constant heat flux can be implemented. The aim of this study is a preliminary visualization of temperature profiles in the reactor, so the simplest model of constant temperatures applied on the walls is used. The influence of the following working parameters on basket temperatures (T_{inf}^{basket}, T_{sup}^{basket}) was studied: coils and reactor wall temperatures (T_{inf}^{cooler}, T_{sup}^{cooler}, T_{inf}^{wall}, T_{sup}^{wall}) and stirring rates (N_{sup}, N_{inf}). Table 4 summarizes the current results of this study.

The first observation is that clear distinct temperatures can be obtained for the two catalytic baskets, with temperature gap ΔT_{basket} going from 2 to 15 K depending on the conditions. It is a first validation of this reactor concept. However the 12-15 K maximum gap observed here could be not enough for several enzymatic/heterogeneous coupled systems, while increase this gap seems very challenging.

The following other conclusions can be taken from Table 4:

- Influence of the coils is largely inferior compared to the reactor walls.
- Magnetic bar stirring rate has a negative but very weak influence.
- Impeller stirring rate has a negative influence. Indeed, stirring rate

Table 4: Series of thermal behavior tests for case 2 (coolers, magnetic bar, Pt/C in upper basket).

Test #	N_{sup} (rpm)	N_{inf} (rpm)	T_{inf}^{cooler} K	T_{sup}^{cooler} K	T_{inf}^{wall} K	T_{sup}^{wall} K	T_{inf}^{basket} K	T_{sup}^{basket} K	ΔT_{basket}
1	1100	300	-	-	323	353	343	347	4
2	1100	300	-	-	303	360	341.8	349	7.2
3	1100	300	-	-	273	360	332.9	344.8	11.9
4	1100	300	-	-	288	360	337.1	347.3	10.2
5	1100	300	-	-	288	368	343.8	352.9	9.1
6	1100	300	-	-	288	353	331.8	341.2	9.4
7	1100	300	288	-	288	368	330.6	341.4	10.8
8	1100	300	288	368	288	368	334.3	346.3	12.0
9	500	300	288	368	288	368	333.5	346.0	12.5
10	1100	600	288	368	288	368	328.1	339.9	11.8
11	1100	600	-	363	273	-	391.2	294.3	3.1
12	1100	600	288	363	-	-	308.5	310.4	1.9
13	1100	600	288	368	288	368	329.3	338.2	9.9
14	1100	300	-	-	263	373	340.8	353.0	12.2
15	600	300	-	-	263	373	330.0	343.3	13.3
16	300	300	-	-	263	373	317.1	331.3	14.2

directly impact mass transfer between lower and upper zone, directly related to heat transfer by convection between the two zones.

- A large temperature gap between cooling and warming temperatures is necessary (80-100 K) to obtain a gap of 10-15 K in the reactor.

Finally to obtain an interesting gap of temperature inside the reactor, heat conditions (double walls and coils) will have to be at their extreme values, experimentally meaning cooling/warming fluid at its lowest/highest possible temperate respectively (273/373 K for water system or 260/383 K for ethylene glycol system). Concerning hydrodynamic conditions, stirring rate should be the lowest, meaning that a compromise between high mass transfer efficiency for reaction (high stirring rate) and low heat convection (low stirring rate) will need to be found.

Figure 14 shows an example of temperature profile inside the reactor. The figure clearly illustrates how two distinct reactor zones are created.

4. Conclusion

During this work a novel double basket reactor designed for hybrid catalysis has been first characterized for its physical transfer properties such as k_La, mixing time and RTD and simulated using CFD. Values of k_La between $0.02\,s^{-1}$ and $0.035\,s^{-1}$ are measured, consistent with values of single basket reactor reported in the literature. The CFD simulation provided the values of velocities in the different parts of the reactor, with velocities reduced in the basket holding the catalysts as expected. The mixing times obtained

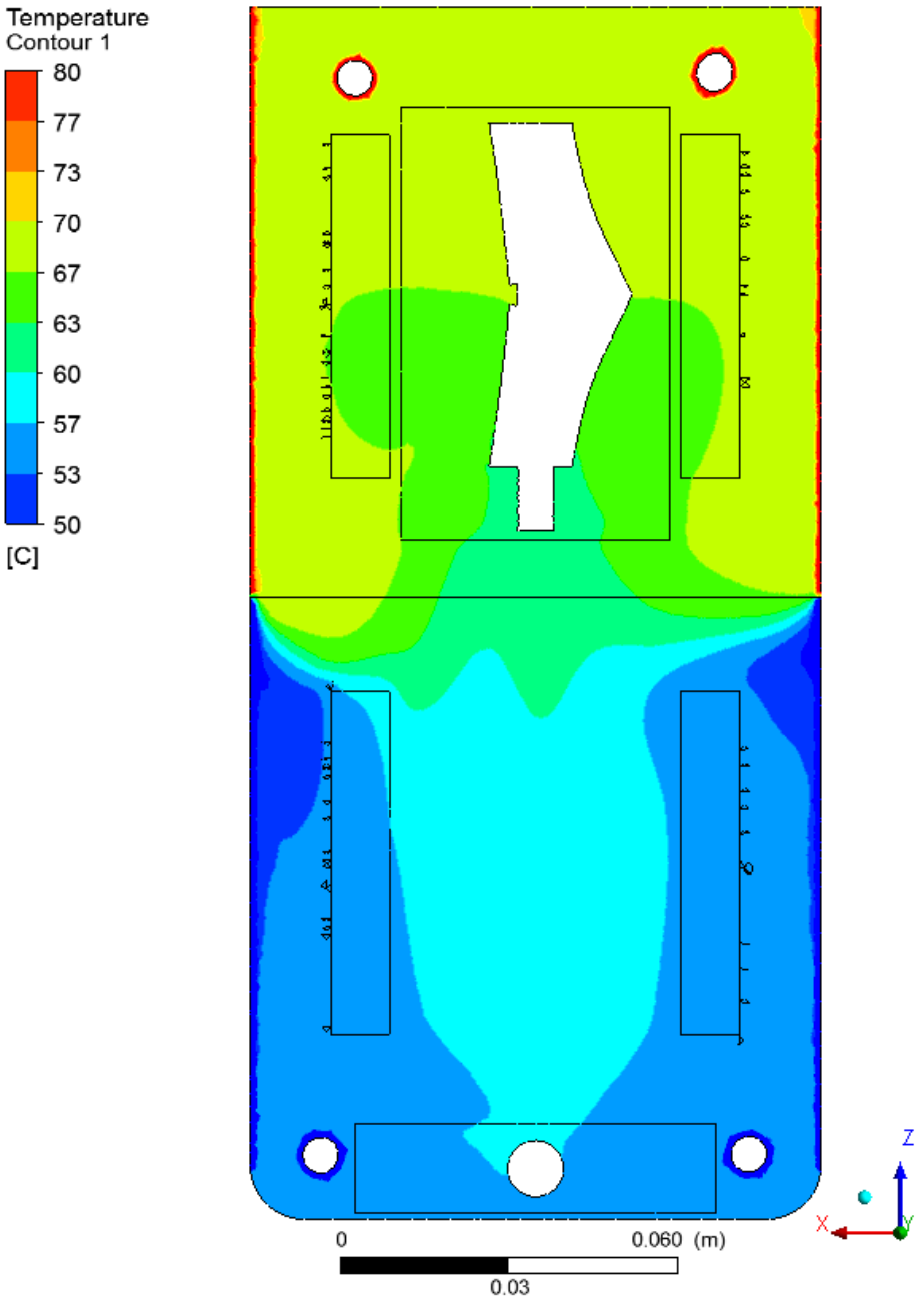

Figure 14: Temperature field in the vertical plan y = 0 for test #11, with temperature in °C.

by simulation have been compared with the experimental ones and the differences discussed. The simulation of the thermal behavior of the reactor showed that it is possible to obtain two zones in the reactor, a *"cold"* one and a *"hot"*, but this could only be achieved by pushing heating conditions to their limits with a very large gap of temperature between the cold and hot sources.

Acknowledgement

This study was carried out in collaboration with SAS PIVERT, as part of the Institute for Energy Transition (ITE) P.I.V.E.R.T (www.institut-pivert.com) selected among the Investments of Future. This study received support from the Investments of Future Program (Reference ANR-001-01).

[1] F. Dumeignil, Hailing the hybrid, Public Serv. Rev. Eur. Union 22 (2011) 528.

[2] F. Dumeignil, Chemical Catalysis and Biotechnology: From a Sequential Engagement to a One-Pot Wedding, Chem. Ing. Tech. 86 (9) (2014) 1496.

[3] H. Gröger, W. Hummel, Combining the 'two worlds' of chemocatalysis and biocatalysis towards multi-step one-pot processes in aqueous media, Current Opinion in Chemical Biology 19 (2014) 171 – 179.

[4] F. R. Bisogno, M. G. López-Vidal, G. de Gonzalo, Organocatalysis and Biocatalysis Hand in Hand: Combining Catalysts in One-Pot Procedures, Advanced Synthesis & Catalysis 359 (12) (2017) 2026–2049.

[5] F. Rudroff, M. D. Mihovilovic, H. Gröger, R. Snajdrova, H. Iding, U. T. Bornscheuer, Opportunities and challenges for combining chemo- and biocatalysis, Nature Catalysis 1 (2018) 12 – 22.

[6] M. Frey, L. Seyidova, D. Richard, P. Fongarland, Hybrid catalysis: study of a model reaction for one-pot reactor combining an enzyme and a heterogeneous catalyst, Catalysis Today In press, corrected proof, (2019) Available online 2 May 2019.

[7] J. Wärnå, M. Ronnholm, T. Salmi, K. Keikko, Application of CFD on a Catalytic Rotating Basket Reactor, Computer Aided Chemical Engineering 10 (2002) 1009 – 1014.

[8] P. Magnico, P. Fongarland, CFD simulations of two stirred tank reactors with stationary catalytic basket, Chem. Eng. Sci. 61 (2006) 1217 – 1236.

[9] V. Santos-Moreau, L. Brunet-Errard, M. Rolland, Numerical CFD simulation of a batch stirred tank reactor with stationary catalytic basket, Chemical Engineering Journal 207-208 (2012) 596–606.

[10] A. Delafosse, M.-L. Collignon, S. Calvo, F. Delvigne, M. Crine, P. Thonart, D. Toye, CFD-based compartment model for description of mixing in bioreactors, Chemical Engineering Science 106 (2014) 76–85.

[11] I. Pitault, P. Fongarland, D. Koepke, M. Mitrovic, D. Ronze, M. Forissier, Gas-liquid and liquid-solid mass transfers in two types of stationary catalytic basket laboratory reactor, Chemical Engineering Science 60 (2005) 6240–6253.

[12] F. Garcia-Ochoa, E. Gomez, Bioreactor scale-up and oxygen transfer rate in microbial processes: An overview, Biotechnology Advances 27 (2009) 153–176.

[13] G. R. Kasat, A. B. Pandit, Mixing Time Studies in Multiple Impeller Agitated Reactors, The Canadian Journal of Chemical Engineering 82 (2004) 892 – 904.

[14] I. Gamba, S. Damian, D. Estenoz, N. Nigro, M. Storti, D. Knoeppel, Residence time distribution determination of a continuous stirred tank reactor using computational fluid dynamics and its application on the mathematical modeling of styrene polymerization., Int. J. Chem. React. Eng. (2012) 10.

[15] G. Micale, M. G., F. Grisafi, A. Brucato, J. Godfrey, CFD simulation of particle distribution in stirred vessels., Chem. Eng. Res. Des. 78 (2000) 435 – 444.

[16] M. Taghavi, R. Zadghaffari, J. Moghaddas, Y. Moghaddas, Experimental and CFD investigation of power consumption in a dual Rushton turbine stirred tank., Chem. Eng. Res. Des. 89 (2011) 280 – 290.

[17] I. Torotwa, C. Ji, A Study of the Mixing Performance of Different Impeller Designs in Stirred Vessels Using Computational Fluid Dynamics., Designs 2 (2018) 10.

[18] L. Raynal, F. Augier, F. Bazer-Bachi, Y. Haroun, C. Pereira Da Fonte, CFD Applied to Process Development in the Oil and Gas Industry - A Review., Oil Gas Sci. Technol. (2016) 71.

[19] Y. Tominaga, T. Stathopoulos, Turbulent Schmidt numbers for CFD analysis with various types of flowfield, Atmospheric Environment 41 (2007) 8091–8099.

[20] J. Aubin, D. Fletcher, C. Xuereb, Modeling turbulent flow in stirred tanks with CFD: The influence of the modeling approach, turbulence model and numerical scheme., Exp. Therm. Fluid Sci. 28 (2004) 431 – 445.

[21] A. Tamburini, A. Cipollina, G. Micale, A. Brucato, M. Ciofalo, CFD simulations of dense solid-liquid suspensions in baffled stirred tanks: Prediction of solid particle distribution., Chem. Eng. J. 223 (2013) 875 – 890.

[22] ANSYS Fluent Theory Guide, Release 18.2., Tech. rep., Ansys Inc. (2017).

[23] ANSYS Fluent User's Guide, Release 18.2., Tech. rep., Ansys Inc. (2017).

[24] A. Karimi, F. Golbabaei, M. R. Mehrnia, M. Neghab, K. Mohammad, A. Nikpey, M. R. Pourmand, Oxygen mass transfer in a stirred tank bioreactor using different impeller configurations for environmental purposes, Iranian Journal of Environmental Health Sciences & Engineering.

[25] A. M. R. Al-Mayah, S. K. Muallah, A. A. Al-Jabbar, Prediction of Oxygen Mass Transfer Coefficients in Stirred Bioreactor with Rushton Turbine Impeller for Simulated (Non-Microbial) Medias, Al-Khwarizmi Engineering Journal, 10 (2014) 1 – 14.

[26] I. Pitault, P. Fongarland, M. Mitrovic, D. Ronze, M. Forissier, Choice of laboratory scale reactors for HDT kinetic studies or catalyst tests, Catalysis Today 98 (2004) 31–42.